First Measurement of Inclusive Muon Neutrino Charged Current Differential Cross Sections on Argon at $E_\nu \sim 0.8$ GeV with the MicroBooNE Detector

C. Adams,[10] M. Alrashed,[12] R. An,[11] J. Anthony,[3] J. Asaadi,[29] A. Ashkenazi,[16] M. Auger,[1] S. Balasubramanian,[34] B. Baller,[9] C. Barnes,[17] G. Barr,[20] M. Bass,[2] F. Bay,[30] A. Bhat,[26] K. Bhattacharya,[21] M. Bishai,[2] A. Blake,[13] T. Bolton,[12] L. Camilleri,[7] D. Caratelli,[9] I. Caro Terrazas,[6] R. Carr,[16] R. Castillo Fernandez,[9] F. Cavanna,[9] G. Cerati,[9] Y. Chen,[1] E. Church,[21] D. Cianci,[7] E. O. Cohen,[27] G. H. Collin,[16] J. M. Conrad,[16] M. Convery,[24] L. Cooper-Troendle,[34] J. I. Crespo-Anadón,[7] M. Del Tutto,[20] D. Devitt,[13] A. Diaz,[16] L. Domine,[24] K. Duffy,[9] S. Dytman,[22] B. Eberly,[8] A. Ereditato,[1] L. Escudero Sanchez,[3] J. Esquivel,[26] J. J. Evans,[15] R. S. Fitzpatrick,[17] B. T. Fleming,[34] D. Franco,[34] A. P. Furmanski,[15] D. Garcia-Gamez,[15] V. Genty,[7] D. Goeldi,[1] S. Gollapinni,[28] O. Goodwin,[15] E. Gramellini,[34, 9] H. Greenlee,[9] R. Grosso,[5] L. Gu,[32] W. Gu,[2] R. Guenette,[10] P. Guzowski,[15] A. Hackenburg,[34] P. Hamilton,[26] O. Hen,[16] C. Hill,[15] G. A. Horton-Smith,[12] A. Hourlier,[16] E.-C. Huang,[14] C. James,[9] J. Jan de Vries,[3] X. Ji,[2] L. Jiang,[22] R. A. Johnson,[5] J. Joshi,[2] H. Jostlein,[9] Y.-J. Jwa,[7] G. Karagiorgi,[7] W. Ketchum,[9] B. Kirby,[2] M. Kirby,[9] T. Kobilarcik,[9] I. Kreslo,[1] I. Lepetic,[11] Y. Li,[2] A. Lister,[13] B. R. Littlejohn,[11] S. Lockwitz,[9] D. Lorca,[1] W. C. Louis,[14] M. Luethi,[1] B. Lundberg,[9] X. Luo,[34] A. Marchionni,[9] S. Marcocci,[9] C. Mariani,[32] J. Marshall,[3, 33] J. Martin-Albo,[10] D. A. Martinez Caicedo,[11, 25] K. Mason,[31] A. Mastbaum,[4] V. Meddage,[12] T. Mettler,[1] J. Mills,[31] K. Mistry,[15] A. Mogan,[28] J. Moon,[16] M. Mooney,[6] C. D. Moore,[9] J. Mousseau,[17] M. Murphy,[32] R. Murrells,[15] D. Naples,[22] P. Nienaber,[23] J. Nowak,[13] O. Palamara,[9] V. Pandey,[32] V. Paolone,[22] A. Papadopoulou,[16] V. Papavassiliou,[18] S. F. Pate,[18] Z. Pavlovic,[9] E. Piasetzky,[27] D. Porzio,[15] G. Pulliam,[26] X. Qian,[2] J. L. Raaf,[9] A. Rafique,[12] L. Ren,[18] L. Rochester,[24] H. E. Rogers,[6] M. Ross-Lonergan,[7] C. Rudolf von Rohr,[1] B. Russell,[34] G. Scanavini,[34] D. W. Schmitz,[4] A. Schukraft,[9] W. Seligman,[7] M. H. Shaevitz,[7] R. Sharankova,[31] J. Sinclair,[1] A. Smith,[3] E. L. Snider,[9] M. Soderberg,[26] S. Söldner-Rembold,[15] S. R. Soleti,[20, 10] P. Spentzouris,[9] J. Spitz,[17] M. Stancari,[9] J. St. John,[9] T. Strauss,[9] K. Sutton,[7] S. Sword-Fehlberg,[18] A. M. Szelc,[15] N. Tagg,[19] W. Tang,[28] K. Terao,[24] M. Thomson,[3] R. T. Thornton,[14] M. Toups,[9] Y.-T. Tsai,[24] S. Tufanli,[34] T. Usher,[24] W. Van De Pontseele,[20, 10] R. G. Van de Water,[14] B. Viren,[2] M. Weber,[1] H. Wei,[2] D. A. Wickremasinghe,[22] K. Wierman,[21] Z. Williams,[29] S. Wolbers,[9] T. Wongjirad,[31] K. Woodruff,[18] W. Wu,[9] T. Yang,[9] G. Yarbrough,[28] L. E. Yates,[16] G. P. Zeller,[9] J. Zennamo,[9] and C. Zhang[2]

(The MicroBooNE Collaboration)[*]

[1]*Universität Bern, Bern CH-3012, Switzerland*
[2]*Brookhaven National Laboratory (BNL), Upton, NY, 11973, USA*
[3]*University of Cambridge, Cambridge CB3 0HE, United Kingdom*
[4]*University of Chicago, Chicago, IL, 60637, USA*
[5]*University of Cincinnati, Cincinnati, OH, 45221, USA*
[6]*Colorado State University, Fort Collins, CO, 80523, USA*
[7]*Columbia University, New York, NY, 10027, USA*
[8]*Davidson College, Davidson, NC, 28035, USA*
[9]*Fermi National Accelerator Laboratory (FNAL), Batavia, IL 60510, USA*
[10]*Harvard University, Cambridge, MA 02138, USA*
[11]*Illinois Institute of Technology (IIT), Chicago, IL 60616, USA*
[12]*Kansas State University (KSU), Manhattan, KS, 66506, USA*
[13]*Lancaster University, Lancaster LA1 4YW, United Kingdom*
[14]*Los Alamos National Laboratory (LANL), Los Alamos, NM, 87545, USA*
[15]*The University of Manchester, Manchester M13 9PL, United Kingdom*
[16]*Massachusetts Institute of Technology (MIT), Cambridge, MA, 02139, USA*
[17]*University of Michigan, Ann Arbor, MI, 48109, USA*
[18]*New Mexico State University (NMSU), Las Cruces, NM, 88003, USA*
[19]*Otterbein University, Westerville, OH, 43081, USA*
[20]*University of Oxford, Oxford OX1 3RH, United Kingdom*
[21]*Pacific Northwest National Laboratory (PNNL), Richland, WA, 99352, USA*
[22]*University of Pittsburgh, Pittsburgh, PA, 15260, USA*
[23]*Saint Mary's University of Minnesota, Winona, MN, 55987, USA*
[24]*SLAC National Accelerator Laboratory, Menlo Park, CA, 94025, USA*
[25]*South Dakota School of Mines and Technology (SDSMT), Rapid City, SD, 57701, USA*
[26]*Syracuse University, Syracuse, NY, 13244, USA*
[27]*Tel Aviv University, Tel Aviv, Israel, 69978*
[28]*University of Tennessee, Knoxville, TN, 37996, USA*
[29]*University of Texas, Arlington, TX, 76019, USA*

[30] *TUBITAK Space Technologies Research Institute, METU Campus, TR-06800, Ankara, Turkey*
[31] *Tufts University, Medford, MA, 02155, USA*
[32] *Center for Neutrino Physics, Virginia Tech, Blacksburg, VA, 24061, USA*
[33] *University of Warwick, Coventry CV4 7AL, United Kingdom*
[34] *Wright Laboratory, Department of Physics, Yale University, New Haven, CT, 06520, USA*
(Dated: May 24, 2019)

We report the first measurement of the double-differential and total muon-neutrino charged-current inclusive cross sections on argon at a mean neutrino energy of 0.8 GeV. Data were collected using the MicroBooNE liquid argon time projection chamber located in the Fermilab Booster neutrino beam, and correspond to 1.6×10^{20} protons on target of exposure. The measured differential cross sections are presented as a function of muon momentum, using multiple Coulomb scattering as a momentum measurement technique, and the muon angle with respect to the beam direction. We compare the measured cross sections to multiple neutrino event generators and find better agreement with those containing more complete physics at low Q^2. The total flux integrated cross section is measured to be $0.693 \pm 0.010 \, (\text{stat.}) \pm 0.165 \, (\text{syst.}) \times 10^{-38} \, \text{cm}^2$.

Current and next generation precision neutrino oscillation experiments aim to probe beyond Standard Model physics, such as CP violation in the lepton sector and sterile neutrinos. These experiments measure the oscillation probability which depends on the neutrino energy, and therefore requires a way to link the energy of reconstructed secondary hadrons and leptons emerging from the neutrino's interaction to its initial energy. This link is complicated by the existence of nuclear effects and final state interactions, which to date cannot be modeled exactly, in particular for heavy target nuclei typically used in modern neutrino experiments. Many future experiments, including DUNE [1–3] and the SBN [4] program, employ liquid argon time projection chambers (LArTPCs) as detectors. As a consequence, neutrino-argon cross section measurements have paramount importance, especially given the relative scarcity of neutrino-argon data [5, 6].

We present the first ν_μ charged-current (CC) inclusive double-differential (in muon momentum and scattering angle) cross section measurement on argon. Neutrinos in the same $\sim 1\,\text{GeV}$ energy range will be studied by the SBND and ICARUS experiments, and this is the energy of the second oscillation maximum for the DUNE experiment. The inclusive CC process, in which only the outgoing muon is required to be reconstructed, comprises multiple interaction processes and is dominantly quasi-elastic scattering in the case of MicroBooNE [7]. Inclusive measurements are particularly important as the clear signal definition allows a straightforward comparison to theory models and other experiments. They are also the foundation for studies of more complex event topologies involving detection of hadrons in the final state. With the fully-active and high-resolution MicroBooNE LArTPC detector, the outgoing muon phase space can be probed with full acceptance in both angle and momentum for the first time. The momentum of the outgoing muon is measured by using multiple Coulomb scattering (MCS) [8] thus allowing the analysis sample to include both exiting and contained muons.

The MicroBooNE detector is located along the Booster Neutrino Beam (BNB) at Fermilab, 463 m from the target. The BNB consists primarily of ν_μ (93.6%) with energy from a few tens of MeV to ~ 2 GeV. In the Micro-BooNE detector [9], charged particles traverse a volume of highly-pure liquid argon leaving trails of ionization electrons along their paths, and also create prompt ultraviolet scintillation photons. Ionization electrons drift in an electric field of 273 V/cm to a system of three anode wire planes located 2.5 m from the cathode plane and are detected by electronics immersed in the liquid argon [10]. Scintillation photons are observed by 32 photomultipliers (PMTs) [11].

The data used in this analysis are taken from an exposure of 1.6×10^{20} protons-on-target (POT), after applying data quality criteria for the beam and detector operating conditions. This corresponds to a four-month exposure, from February to July 2016. Two different data streams are used in this analysis: an on-beam data sample, triggered by BNB neutrino spills; and an off-beam data sample, taken during periods when no beam was received. The off-beam data sample is used for a data-driven measurement of cosmic ray (CR) backgrounds, which is important because the MicroBooNE detector operates on the Earths surface.

The flux of neutrinos at the MicroBooNE detector is simulated using the framework built by the Mini-BooNE collaboration [12]. Neutrino interactions in the MicroBooNE detector are simulated using the GENIE event generator [13], which generates the primary neutrino interaction inside the nucleus, the production of all final-state particles in the nucleus (hadronization), and the transport and rescattering of the final-state particles through the nucleus (final state interactions). CRs crossing the detector volume within the readout window of neutrino events are simulated with CORSIKA [14]. The simulation of the MicroBooNE detector is based on GEANT4 [15] and includes particle propagation, drift of ionization electrons to the wire planes, as well as propagation of scintillation light to the PMTs. All simulation

is carried out within the LArSoft framework [16].

Data processing begins with a requirement that PMT activity occurs in coincidence with the arrival of neutrinos, which results in a negligible loss of signal. TPC waveforms originate from drift electrons inducing bipolar signals on the first two wire planes and a unipolar signal on the last plane, which collects the electrons. A noise filtering algorithm removes inherent and electronic noise [10], and the signals are deconvolved to a Gaussian to further eliminate detector artifacts [17]. Individual signal waveforms are identified as hits and are sorted spatially to form clusters. Clusters are matched across planes and identified as track-like or shower-like by the Pandora multi-algorithm pattern recognition framework [18]. Optical reconstruction combines correlated PMT waveforms across the detector into flashes.

A series of algorithms is used to identify and remove CRs. These algorithms identify tracks that traverse the detector from top to bottom, adding optical information to identify CRs that enter from the anode or cathode planes. Stopping muon tracks originating outside the detector are identified as CRs either by their Bragg peak or by their Michel decay.

This analysis makes use of the optical system to further use the flash identified in the 1.6 μs beam window, which is in coincidence with the beam spill, matching it to an ensemble of TPC tracks and showers originating from a common vertex. This matching is crucial to the mitigation of the high CR rate. Calorimetric information in the form of a truncated mean value of the deposited charge per unit length, dQ/dx, and track length, are used to discriminate muons from protons. The candidate interaction must contain a track that has a measured dQ/dx compatible with a muon. If more than one track is present, the longest track is selected as the muon candidate. Several algorithms ensure the quality of the fitted track by limiting the allowed spatial dispersion of the reconstructed hits with respect to the track hypothesis.

The momentum of the muon is measured using Multiple Coulomb Scattering. Here, the magnitude of the momentum is a fit parameter that describes the scattering pattern of the track [8]. The strength of this algorithm is that it can estimate the muon momentum for muon tracks spatially contained in the detector as well as exiting tracks. In addition, the measured momentum using MCS for contained tracks is used to identify and exclude mis-reconstructed tracks from the analysis by comparing the MCS momentum to the momentum estimate from the track's range. The two would disagree if the reconstructed track is incomplete or inaccurate.

Figure 1 shows the measured vs. generated muon momentum p_μ and the measured vs. generated $\cos\theta_\mu$ for simulated events, where θ_μ is the muon angle with respect to the incident neutrino beam direction. There is a possibility for tracks to be mis-reconstructed with the opposite direction [18]. The impact is strongest in the two backwards bins, $\cos\theta_\mu \in [-1, -0.5]$ and $\cos\theta_\mu \in [-0.5, 0)$, where 46% and 56% of events come from the same bin they were generated in, respectively. The other events are actually forward going but get reconstructed with the opposite direction [18]. This effect is included in the smearing matrix and muon kinematic distributions of data and simulation remain comparable with each other.

The final selected sample contains 27,200 events. The signal selection efficiency, measured in simulation, is 57.2%. The selection accepts events across the entire angular phase space. The purity of the final selection is 50.4%. The efficiency and purity are relatively flat as a function of muon kinematics and the number of final state particles. Different interaction processes have approximately the same efficiency. The main backgrounds in this analysis are: (i) CRs that overlap in-time with the beam spill and trigger the readout (estimated to be 29.1% of all selected events); (ii) CRs overlaid with neutrino interactions in which the cosmic muon was misidentified as coming from a neutrino interaction (6.4%); (iii) neutrinos that interact outside the fiducial volume with an entering track selected as the muon candidate (7.6%); (iv) events in which a neutrino interacts outside the cryostat but the muon enters the TPC and is selected (here called "dirt" interactions) (4.4%); (v) neutral current interactions where a final state particle is misidentified as a muon (1.6%); (vi) beam intrinsic muon antineutrino interactions (0.4%); and (vii) beam intrinsic electron (anti-)neutrino interactions (0.1%). The largest background (i) is measured with off-beam data and subtracted from the on-beam data. The off-beam data sample has twice the statistics of the on-beam data. Other backgrounds are estimated from simulation. The accuracy of the detector modeling has been verified by looking at selected event distributions of variables not affected by the neutrino interaction physics, e.g., the interaction points in the detector, where we have good data to simulation agreement.

This analysis measures the double-differential ν_μ CC cross section on argon as a function of the muon momentum p_μ (measured using MCS) and the cosine of the muon angle θ_μ with respect to the beam direction. The flux-integrated, double-differential cross section measured in bin i is defined as:

$$\left(\frac{d^2\sigma}{dp_\mu d\cos\theta_\mu}\right)_i = \frac{N_i - B_i}{\tilde{\epsilon}_i \cdot T \cdot \Phi_{\nu_\mu} \cdot (\Delta p_\mu \cdot \Delta\cos\theta_\mu)_i}, \quad (1)$$

where N_i, B_i and $\tilde{\epsilon}_i$ are the number of selected data events, the expected background events, and the detection efficiency in bin i. $(\Delta p_\mu \cdot \Delta\cos\theta_\mu)_i$ is the ith bin area. T and Φ_{ν_μ} are the number of target nucleons, and the integrated BNB muon-neutrino flux from 0 to 10 GeV. The total integrated BNB ν_μ flux in neutrino mode running, corresponding to 1.6×10^{20} POT, is $\Phi_{\nu_\mu} = 1.16 \times 10^{11}\ \nu_\mu/\text{cm}^2$, and its mean neutrino energy
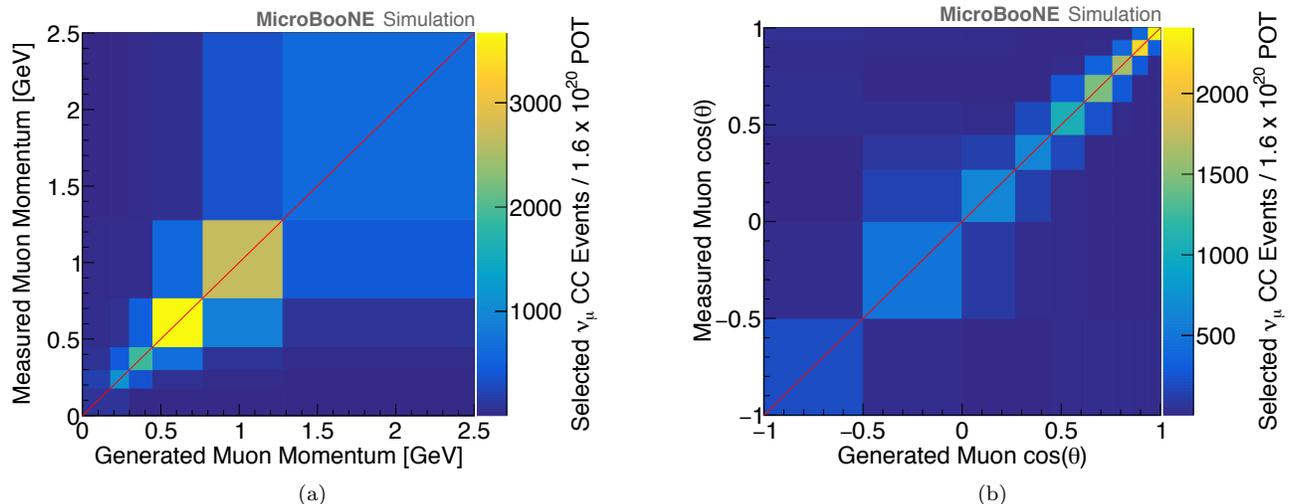
(a)

(b)

FIG. 1. Comparison of the generated vs. measured muon momentum (a) and cosine of the muon angle (b) for the simulated and selected ν_μ CC events. The binning is the same as used in the cross-section extraction.

is 823 MeV. The relevant energy range for this measurement is from 325 to 1325 MeV, which includes 68% of neutrinos from the BNB.

We report the final cross section result as a function of measured kinematic variables following a "forward-folding" approach. This is done using a migration matrix S, which transforms the number of generated events N_j^{gen} in a bin j of generated momentum and angle to the number of events N_i in a bin i of measured momentum and angle. $N_i = \sum_{j=1}^{M} S_{ij} N_j^{\text{gen}}$ where S is given by $S_{ij} = P(\text{measured in bin } i \,|\, \text{generated in bin } j)$ and M is the total number of bins. The efficiency used in Eq. (1) as a function of the measured quantities, $\tilde{\epsilon}_i$, is given by

$$\tilde{\epsilon}_i = \frac{\sum_{j=1}^{M} S_{ij} N_j^{\text{sel}}}{\sum_{j=1}^{M} S_{ij} N_j^{\text{gen}}}, \qquad (2)$$

where N_j^{sel} and N_j^{gen} are the number of selected and generated signal events in bin j, respectively, with j being a bin in generated momentum and angle.

The uncertainty on the measurement is dominated by systematic uncertainties, which come from the neutrino flux, neutrino interaction model, and detector response. Uncertainties, both statistical and systematic, are encoded in a covariance matrix, E. The total uncertainty matrix is a combination of the statistical and systematic errors, $E = E^{\text{stat}} + E^{\text{syst}}$, where E^{stat} is the statistical uncertainty matrix, and E^{syst} is the systematic covariance matrix.

To assess the uncertainties on the neutrino flux prediction, the final flux simulation from the MiniBooNE collaboration is utilized [12], updated to the MicroBooNE detector location. For neutrino cross section modeling uncertainties, we use the GENIE framework of event reweighting [13, 19] with its standard reweighting param-

TABLE I. Contributions to the total cross section systematic uncertainty.

Source of uncertainty	Relative uncertainty [%]
Beam flux	12.4
Cross section modeling	3.9
Detector response	16.2
Dirt background	10.9
Cosmic ray background	4.2
MC statistics	0.2
Stat	1.4
Total	23.8

eters. For both cross section and flux systematics we use a *multisim* technique [20], which consists of generating several MC replicas, each one called a "universe", where parameters in the models are varied within their uncertainties. Each universe represents a different reweighting. N such universes are then created that can be combined to construct the covariance matrix:

$$E_{ij} = \frac{1}{N} \sum_{n=1}^{N} (\sigma_i^n - \sigma_i^{cv})(\sigma_j^n - \sigma_j^{cv}), \qquad (3)$$

where σ is a shorthand notation for the double-differential cross section in Eq. (1), i and j correspond to bins in measured quantities, σ_i^{cv} is the central value cross section in bin i, and σ_i^n is the cross section evaluated in the systematic universe n.

A different model is followed for systematics associated with the detector model. In this case *unisim* samples [20] are generated, where only one detector parameter at a time is changed by its uncertainty. For M detector pa-
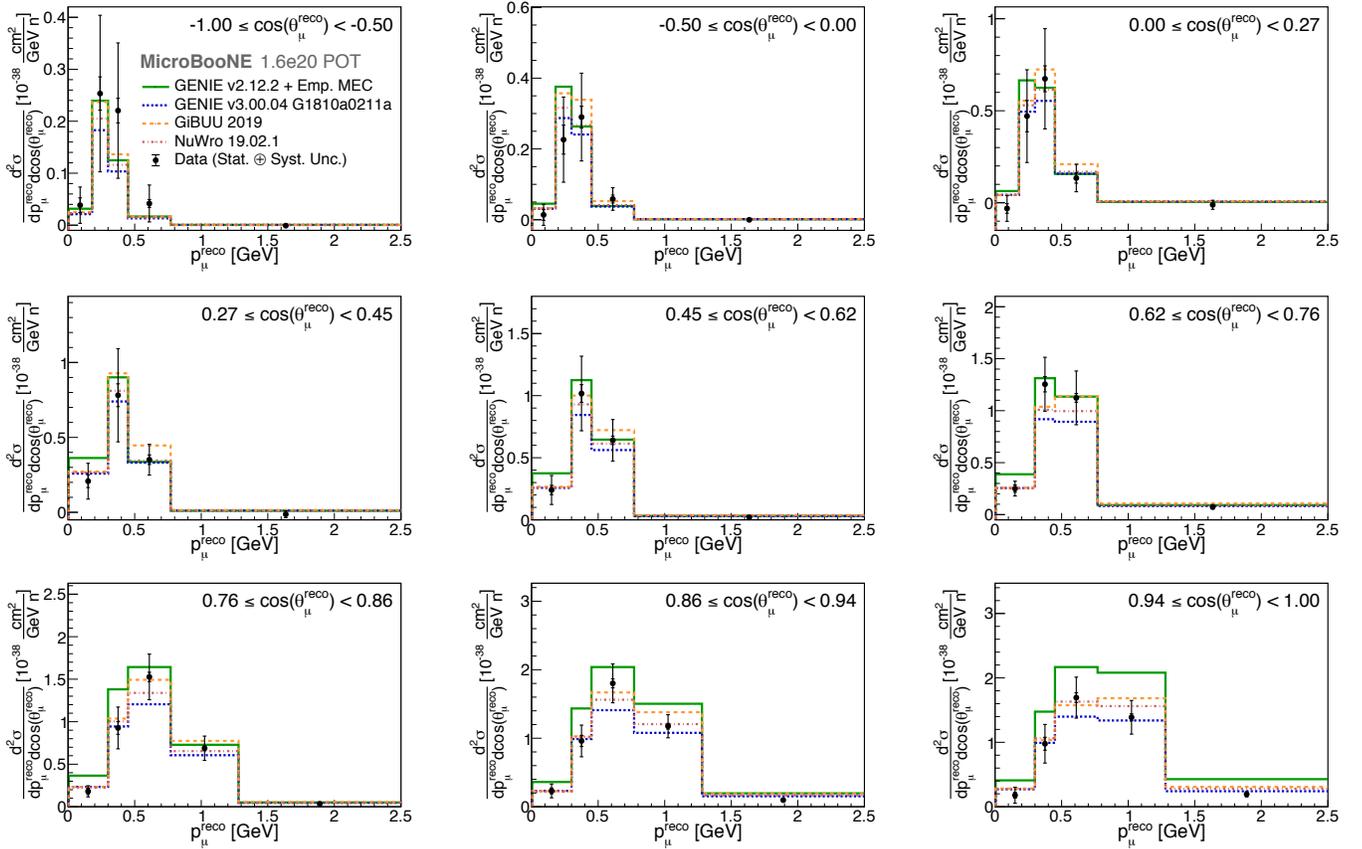
FIG. 2. ν_μ CC inclusive double-differential cross section on argon per nucleon n as a function of the measured muon momentum and cosine of the measured muon polar angle (angle with respect to the incoming neutrino direction). The data (black) is compared to a GENIE v2 with empirical MEC prediction (green), a GENIE v3 prediction (blue), a GiBUU prediction (orange), and a NuWro prediction (red), as described in the text. The vertical bars show statistical and systematic uncertainties.

rameters, the covariance matrix is

$$E_{ij} = \sum_{m=1}^{M} (\sigma_i^m - \sigma_i^{cv})(\sigma_j^m - \sigma_j^{cv}). \qquad (4)$$

The total flux, cross section, and detector uncertainties amount to 12%, 4%, and 16% of the total cross section, respectively. The largest individual contribution to the detector uncertainty comes from using a simple model to simulate the induced charge on neighboring wires of the TPC, leading to a 13% uncertainty on the total cross section. Additional uncertainties are assessed on the dirt and simulated CR background interactions overlaying neutrino interactions, which yield 11% and 4% uncertainties on the final cross section measurement, respectively. A summary of systematic uncertainty is shown in Table I.

The double-differential cross section is presented in Fig. 2 and compared with several predictions from different generators. The first uses the default GENIE configuration in GENIE v2.12.10, with the addition of a Meson Exchange Current (MEC) interaction channel modeled with an empirical approach [21]. We also compare to a

more recent version of GENIE – v3.0.4 – in which we use the G18_10a_02_11a comprehensive model configuration. This includes a number of theoretically motivated improvements. It replaces the Bodek-Ritchie Fermi Gas nuclear model with a Local Fermi Gas (LFG) for the nuclear initial state. The Valencia model is used for quasi-elastic and MEC interactions [22, 23], and the Kuzmin-Lyubushkin-Naumov [24] and Berger-Seghal [25] model with form factors from MiniBooNE data [26] for resonant pion production. We also compare to predictions from NuWro and GiBUU. NuWro 19.02.1 [27] uses a similar set of models to the GENIE v3.0.4 configuration, though the resonant pion production form factors are modified [28] and the final state interaction model is the Oset intranuclear cascade model [29]. GiBUU 2019 [30] has consistent nuclear medium corrections throughout. It also uses a LFG model to describe the nucleon momenta, a separate MEC model [30], and propagates final state particles according to the Boltzmann-Uehling-Uhlenbeck transport equations.

This is the first test of neutrino event generators against double differential neutrino scattering data on

argon. As is also seen in comparisons to neutrino data on carbon [31, 32], high χ^2 values between data and predictions is observed taking into account the full covariance matrix with off diagonal elements (not displayed in Fig. 2). The largest disagreements between the data and predictions are observed in the high-momentum bins in the most forward-going muon angular bins of $0.94 \leq \cos(\theta) \leq 1$ and $0.86 \leq \cos\theta < 0.94$. This region strongly disfavors the GENIE v2 with empirical MEC, while other predictions show less tension with the data in the highest momentum bin with the angular range of $0.94 \leq \cos(\theta) \leq 1$, but not for $0.86 \leq \cos\theta < 0.94$. The lowest χ^2 value is obtained for the GENIE v3 model with a χ^2 of 108.8 for 42 bins. The reduced tension originates from the overall reduced cross section in the forward region when adopting the Local Fermi Gas nuclear initial state, which is expected to be a more realistic momentum distribution of the initial state nucleons, and to a lesser extent the RPA correction as included in the GENIE v3 and NuWro predictions. These effects have the largest impact at low neutrino energies and for heavy nuclear targets, which explains why MicroBooNE is more sensitive to these effects than previous experiments. For this reason, these new MicroBooNE cross section results are very valuable for addressing and testing the details of the current neutrino cross section models and for making progress in understanding the physics associated with neutrino interactions.

Additionally, we compute a flux-integrated cross section $\sigma(\nu_\mu + \text{Ar} \rightarrow \mu^- + X)$ per nucleon of

$$\sigma = 0.693 \pm 0.010\,(\text{stat.}) \pm 0.165\,(\text{syst.}) \times 10^{-38}\,\text{cm}^2, \quad (5)$$

which is obtained by integrating the number of signal and background events, as well as the efficiency over all bins.

In summary, we have reported the first double-differential ν_μ charged-current inclusive cross section on argon. The presented analysis has full angular coverage and uses multiple Coulomb scattering to estimate the muon momentum, a significant step forward for the LArTPC technology.

As shown in the comparison with various predictions, these data provide a way to differentiate models in neutrino event generators. These measurements not only inform the theory of neutrino-nucleus scattering, but also reduce the systematic uncertainties associated with cross section measurements in neutrino oscillation experiments.

––––––––––––

* microboone_info@fnal.gov

[1] B. Abi *et al.* (DUNE Collaboration), The DUNE Far Detector Interim Design Report Volume 1: Physics, Technology and Strategies (2018), arXiv:1807.10334.

[2] B. Abi *et al.* (DUNE Collaboration), The DUNE Far Detector Interim Design Report, Volume 2: Single-Phase Module (2018), arXiv:1807.10327.

[3] B. Abi *et al.* (DUNE Collaboration), The DUNE Far Detector Interim Design Report, Volume 3: Dual-Phase Module (2018), arXiv:1807.10340.

[4] M. Antonello *et al.* (LAr1-ND, ICARUS-WA104, MicroBooNE Collaborations), A Proposal for a Three Detector Short-Baseline Neutrino Oscillation Program in the Fermilab Booster Neutrino Beam (2015), arXiv:1503.01520.

[5] R. Acciarri *et al.* (ArgoNeuT Collaboration), Phys. Rev. **D89**, 112003 (2014).

[6] C. Anderson *et al.* (ArgoNeuT Collaboration), Phys. Rev. Lett. **108**, 161802 (2012).

[7] J. A. Formaggio and G. P. Zeller, Rev. Mod. Phys. **84**, 1307 (2012).

[8] P. Abratenko *et al.*, JINST **12**, P10010 (2017).

[9] R. Acciarri *et al.* (MicroBooNE Collaboration), JINST **12**, P02017 (2017).

[10] R. Acciarri *et al.* (MicroBooNE Collaboration), JINST **12**, P08003 (2017).

[11] J. Conrad, B. Jones, Z. Moss, T. Strauss, and M. Toups, JINST **10**, T06001 (2015).

[12] A. A. Aguilar-Arevalo *et al.* (MiniBooNE Collaboration), Phys. Rev. **D**, 072002 (2009).

[13] C. Andreopoulos *et al.*, Nucl. Instrum. Meth. **A**, 87, version 2_12_2 (2010).

[14] D. Heck, J. Knapp, J. Capdevielle, G. Schatz, and T. Thouw, Forschungszentrum Karlsruhe Report FZKA, version 7.4003 with constant mass composition model (1998).

[15] S. Agostinelli *et al.*, Nucl. Instrum. Meth. **506**, 250 (2003).

[16] R. Pordes and E. Snider, PoS ICHEP **182** (2016).

[17] B. Baller, JINST **12**, P07010 (2017).

[18] R. Acciarri *et al.* (MicroBooNE Collaboration), Eur. Phys. J. **C78**, 1 (2018).

[19] C. Andreopoulos *et al.*, The GENIE Neutrino Monte Carlo Generator: Physics and User Manual (2015), arXiv:1510.05494.

[20] B. P. Roe, Nucl. Instrum. Meth. **570**, 159 (2007).

[21] T. Katori, AIP Conf. Proc. **1663**, 030001 (2015).

[22] J. Nieves, I. R. Simo, and M. J. V. Vacas, Phys. Rev. C **83**, 045501 (2011).

[23] R. Gran, J. Nieves, F. Sanchez, and M. J. V. Vacas, Phys. Rev. D **88**, 113007 (2013).

[24] K. S. Kuzmin, V. V. Lyubushkin, and V. A. Naumov,

Mod. Phys. Lett. A **19**, 2815 (2004).

[25] C. Berger and L. M. Sehgal, Phys. Rev. D **79**, 053003 (2009).

[26] J. A. Nowak, AIP Conf. Proc. 1189 **1**, 243 (2009).

[27] T. Golan, J. Sobczyk, and J. Zmuda, Nuclear Physics B - Proceedings Supplements **229-232**, 499 (2012).

[28] K. M. Graczyk, D. Kiełczewska, P. Przewłocki, and J. T. Sobczyk, Phys. Rev. D **80**, 093001 (2009).

[29] L. Salcedo, E. Oset, M. Vicente-Vacas, and C. Garcia-Recio, Nuclear Physics A **484**, 557 (1988).

[30] O. Buss *et al.*, Physics Reports **512**, 1 (2012).

[31] D. Ruterbories *et al.* (MINERvA), Phys. Rev. **D99**, 012004 (2019), arXiv:1811.02774 [hep-ex].

[32] K. Abe *et al.* (T2K), Phys. Rev. **D98**, 012004 (2018), arXiv:1801.05148 [hep-ex].